PAPER

Check for updates

Facile synthesis and self-assembly of pharmaceutically important oligobenzylidene-D-sorbitol dialdehydes: direct encapsulation and stimuli responsive delivery of H₂S†

Vara Prasad Rebaka, Yogendra Kumar, Tohira Banoo, Arun Kumar Rachamalla and Subbiah Nagarajan (ID) *

Over the past two decades, the development of stimuli-responsive drug delivery materials for healthcare applications has drawn significant attention. A detailed investigation of one of the critical endogenously produced gaseous molecules, H_2S, revealed its significance in promoting tissue regeneration, angiogenesis, organelle function, stress and antioxidant effect. Even though a continuous delivery of H_2S can suppress cancer cell progression, its administration as a therapeutic drug has become highly challenging because of its gaseous nature and reactivity. By considering the limitations of the existing H_2S delivery, we have developed a smart, biocompatible drug delivery system for the direct delivery of H_2S from bio-based resources. In this report, we have synthesized oligo[1,3:2,4-(O-benzylidene)-D-sorbitol]-dialdehyde (OBSDA) using an FDA-approved GRAS chemical and environmentally benign protocol in good yields. The ability of OBSDA to self-assemble into supramolecular gels was systematically studied in a broad range of solvents. To our fortune, OBSDA displayed gelation in N-methyl pyrrolidone (NMP), one of the FDA-approved solvents displaying a well-established safety profile and anti-inflammatory properties. Molecular level interactions responsible for the formation of the supramolecular gels have been identified using NMR and FTIR analysis. The self-assembly, mechanism, morphology and strength of the gel were systematically studied using XRD, scanning electron microscopy and rheological studies. For the first time, we report the direct *in situ* encapsulation of H_2S into the gel formed by using a pharmaceutical solvent, NMP, by gaining input from the Purisol process. A stimuli-responsive delivery of encapsulated H_2S *via* gel-to-sol transition has been achieved by the addition of acidic buffer. The reported precise delivery will enable future studies of the physiological role of H_2S in various biological processes.

Introduction

Supramolecular chemistry refers to "chemistry beyond molecules," which largely focuses on high-order assemblies and molecular reorganization by means of non-covalent interactions.[1] Indeed, supramolecular chemistry involved in biological systems often renders inspirational concepts to the scientists to develop advanced smart materials. In particular, modern and efficient drug delivery systems involving the concept of supramolecular chemistry, such as molecular self-assembly, molecular recognition, and foldamers, receive greater attention and render a finite solution for the

treatment of various diseases.[2] Generally, these systems deliver active pharmaceutical ingredients like drugs, enzymes, peptides, vaccines and nutrients to a specific target in the body for an extended period of time at a controlled rate. The main advantages of supramolecular delivery systems, generally referred to as nanomedicine, include reduced side effects, controlled dosage, increased bio-availability, improved solubility and efficiency of the drug with broad administration methods.[3] In pharmaceutical formulations, various drug delivery systems including liposomal formulations,[4] micelles,[5] nanoparticles,[6] implantable systems,[7] biopolymers,[8] and low molecular weight gels,[9] have been used for treating various diseases. In particular, clinical trials have shown that nanomedicine is pharmacologically and pharmacokinetically more efficient than the drug-alone formulation.[10] It is worth mentioning that over 100 nanomedicine-based formulations have been approved by the US Food and Drug Administration (FDA)

Assembled Organic & Hybrid Materials Research Lab, Department of Chemistry, National Institute of Technology Warangal, Hanumakonda-506004, Telangana State, India. E-mail: snagarajan@nitw.ac.in

† Electronic supplementary information (ESI) available. See DOI: https://doi.org/10.1039/d3ma01110k

and the European Medical Agency (EMA). Doxil®, Somavert®, Avinza®, Venofer®, and Abraxane® are the representative examples of commercial lipid, polymer, nanocrystal, inorganic nanoparticle, and protein-based nanomedicine, respectively.[11] In order to meet the high pharmaceutical market demand, there is a rapid growth in research and development of nanomedicine-based advancements.

H_2S, also known as sewer gas or swamp gas with a rotten egg odour, displays corrosiveness, flammability and toxicity. It is recognised as one of the industrial and environmental toxicants.[12] In 1996, Abe and Kimura reported that the physiological concentration of H_2S selectively enhances the N-methyl-D-aspartate (NMDA) receptor-mediated responses and thus is actively involved in the modulation of synaptic activities regulated by hormones and neurotransmitters.[13] Since then, H_2S has been widely explored for a vast array of physiological functions of the cardiovascular, gastrointestinal, excretory, nervous and immune systems.[14] Recent research reveals the potential of H_2S in the treatment of Alzheimer's, arthritis, strokes, Parkinson's and diabetes owing to its anti-inflammatory, antioxidant, proangiogenic and anti-apoptotic properties.[15–19] Generally, endogenous generation of H_2S is effective in carrying out various physiological functions including dietary restriction benefits.[20] Direct administration of exogenous sulfide in gaseous or salt form rapidly increases its concentration in the blood, which leads to adverse effects; hence the development of drugs releasing H_2S in a controlled way is quite challenging.[21] The ideal drug delivery system should release H_2S in a controlled manner triggered by a specific response. So many attempts have been made to develop H_2S delivery systems using nanomedicine concepts (Table S1, ESI†).[22–30] However, the reported methods displayed various limitations, such as tedious synthetic procedures, less loading capacity, biocompatibility and a complex delivery mechanism (Table S1, ESI†).

Among the various nanomedicine-based delivery systems, gels formed by low molecular weight gelators have attracted a broad range of interest because of their 3D-porous network, extensive loading capability, ease of tunability, biocompatibility and stimuli responsiveness.[22] Low molecular weight gels are 3D network structures obtained by bottom-up assembly of small molecules using various intermolecular interactions such as H-bonding, π–π, anionic–π, cationic–π, halogen–π interactions and van der Waals forces, which are capable of immobilizing solvents through surface tension and capillary forces.[31] Gels derived from small molecules render exciting architectures with unconventional coalesce of properties, which is different from solids, liquids and gases. Because of their fascinating specific physical and chemical properties, gels have applications in cell culture and release, optoelectronics, polymorph control, water purification, drug loading and delivery, and food industries.[32] The ready reversibility of gels with respect to the environment enables them to behave like a smart material, where supramolecular manipulations can be triggered by external stimuli.

Matson and co-workers have developed a hydrogel using S-aroylthiooxime conjugated peptides, which can deliver H_2S by the decomposition of the S-aroylthiooxime moiety.[33–37] Liang et al. have generated an H_2S prodrug by grafting 2-aminopyridine-5-thiocarboxamide on partially oxidized alginate, which upon decomposition releases H_2S endogenously.[38] Recently, Nagarajan and co-workers have developed an enolizable amphiphilic gel from renewable resources and used it for the direct delivery of H_2S, wherein the reaction of Na_2S and water generated H_2S.[39] Hyaluronic acid-based hydrogel has been used as a matrix for encapsulating H_2S donors, which are released through pH response for repairing wounds on skin.[40] In the recent past, various polymer conjugated H_2S prodrugs, such as dithiolethiones (DTTS), aryl thioamides, acyl protected perthiols, dialkyl trisulfide, dialkyl tetrasulfide, polysulfides, N-benzoylthiobenzamides N-thiocarboxyanhydrides, Na_2S, S-aroylthiooximes (SATOs), Lawesson reagents (phosphonamidodithiolates), geminal dithiols, thioether ketones, thiocarbamates, tarbanothioates and carbamothioates, have been developed.[41] However, controlled release is achieved by a complex chemical/enzymatic process. The main reason for the evolution of the prodrug concept in H_2S delivery is because of the poor encapsulation of H_2S in solid, liquid and gel phases. A careful analysis of the molecular structure of the H_2S prodrug and the release mechanism shows that the overall release of H_2S would be very low. In order to achieve the desired concentration of H_2S release, a huge amount of H_2S prodrug loading is necessitated.

In order to overcome the existing limitations, we have developed an oligo[1,3:2,4-(O-benzylidene)-D-sorbitol]-dialdehyde (OBSDA) based organogelator as a H_2S drug delivery system. The idea of developing OBSDA originated from 1,3:2,4-di-(O-benzylidene)-D-sorbitol (DBS), which is one of the well-known chiral amphiphiles prone to form a gel in a broad range of solvents for over a century. In particular, DBS-based gelators have gained attention among researchers because of their biocompatibility, facile bottom-up assembly in a broad range of solvents, multi-functionality and multi-responsive behaviour.[42]

For the synthesis of OBSDA, we have used sorbitol as one of the starting materials because of its natural abundance, biodegradability, biocompatibility and eco-friendliness. Sorbitol is a sugar substitute providing dietary energy with an E number of E420 and is also classified as generally recognised as safe (GRAS) by the FDA. Sorbitol is often used in medicine, health care, food and cosmetics.[43] Another starting material, terephthalaldehyde, used for the synthesis of OBSDA facilitates π–π stacking interactions. In this report, we have synthesized OBSDA from biologically significant starting materials using a simple protocol in good yield. Bottom-up assembly of OBSDA in polar solvent furnished a 3D network structure, wherein the polar solvents are trapped. To our fortune, OBSDA formed a gel in N-methyl pyrrolidone (NMP), a widely used pharmaceutical solvent displaying bioactive and anti-inflammatory properties. In addition, NMP is a widely preferred solvent for solubilizing many commercial drugs and it has the tendency to enhance the drug penetration in humans as well as animals.[44] The famous Purisol process is adopted in petrochemical industries to selectively remove H_2S from syn gas using NMP solvent.[45] Inspired by the Prusiol process, we have directly encapsulated

H2S in the OBSDA gel formed in NMP solvent and demonstrated controlled stimuli-responsive delivery. A plausible self-assembly and pH as a stimuli-responsive H2S release mechanism have been investigated. This is the first report on the direct encapsulation of H2S in a low molecular weight gel system comprising biologically significant materials.

Results and discussion

DBS gels derived from sorbitol display potential applications in pharmaceuticals, food industries, and personal care products. In pharmaceuticals, DBS-based gels act as a stimuli-responsive drug delivery system for the controlled release of naproxen, rosuvastatin, ibuprofen and mesalazine.[46–48] In continuation of our ongoing research in the field of fabrication of assembled organic materials and also by considering the potential application of DBS, we envisioned to synthesize an analogue of DBS, *i.e.* OBSDA, using a simple protocol. The chemistry of hydroxyl functionalization of monosaccharides has been prevalent over 100 years of history and displays a bright future because of displaying high-tech applications such as environmental remediation, tissue engineering, and the fabrication of optical and electronic materials. The chemistry of OBSDA synthesis is in a similar line with DBS, where the formation of acetal is the key step. Traditionally, Lewis acids such as $AlCl_3$, $ZnCl_2$, $SnCl_2$, $FeCl_3$ and BF_3, and Brønsted acids such as *p*-toluenesulfonic acid, phosphoric acid, *etc.* were typically used for the formation of sugar acetal.[49] An extensive literature search revealed that the use of Brønsted acids in excess during the reaction lowers the yield by forming impurities and enhances the purification process. In addition, the use of metal-based Lewis acids allows traces of metal ions in the product because of the strong interaction of sugar acetals with metal ions, which limits its applications on an industrial scale. Even though DBS is commercially available, the reported procedure for the synthesis of DBS did not work well in the case of OBSDA, because of the involvement of simultaneous formation of more than two acetals. In the process of identifying suitable reaction conditions to synthesize OBSDA (3–6) in good yield, we have selected various Lewis and Brønsted acids as a catalyst and a broad range of solvents. Based on the literature, our initial attempts with the use of 0.2 mol% of Lewis acids such as $AlCl_3$, $ZnCl_2$, $SnCl_2$, $FeCl_3$ and $BF_3 \cdot OEt_2$ as catalysts in MeCN at rt furnished tetrabenzylidene-disorbitol (3) in low to moderate yields (31–67%). In carbohydrate chemistry, it is well known that the use of Brønsted acids can facilitate acetal formation by the protonation of the carbonyl group of the aldehyde followed by the attack of a hydroxyl nucleophile. Among the various Brønsted acids used, *p*-TSA rendered tetrabenzylidene-disorbitol (3) in moderate yield (55%). To our surprise, the use of heterogeneous catalysts such as Dowex and Amberlyst at room temperature furnished HBSD 4 with 72 and 78% yield, respectively (Table 1). In order to enforce the reaction, the reactivity of all the catalysts was studied at elevated temperature and prolonged reaction time. Unfortunately, the Lewis acids selected for the

investigation did not render a satisfactory result. From careful analysis of the reaction mechanism of acetal formation in sorbitol, metal ions in the Lewis acid are entrapped in the benzylidene sorbitol moiety by means of weak van der Waals forces, and hence are not readily available for the further activation of the carbonyl group of pendent aldehyde groups. It is worth mentioning that there is no further progress of the reaction in the case of increasing mol% of Lewis acid. Subsequently, acetal formation in sorbitol using terephthaldehyde in heterogeneous catalysts at 50 °C delivered encouraging results. It is noteworthy to mention that the reaction at elevated temperature furnishes higher analogues of the benzylidene sorbitol product.

Having optimized the catalysts, Dowex and amberlyst, the increase in temperature and time render HBSD **4** and OBSD **5**. The change of solvents did not provide satisfactory results. Altogether, the use of heterogeneous catalysts such as Dowex and amberlyst at different temperatures and varying times can furnish one of the TBSD, HBSD or OBSD as a major product.

During the progress of the reaction, the acetal product formed is separated as a precipitate or gelatinous substance. After completion of the reaction as identified by TLC, the precipitate is dissolved in a hot cyrene solvent, and the heterogeneous catalyst is separated by filtration. The cyrene solution containing the desired compound is kept under refrigeration for crystallization. The yield denoted in Table 1 is after recrystallization. In order to identify the number of oligomeric units formed during the reaction, ^{1}H-NMR and mass spectral techniques were used. Altogether, we were able to synthesize OBSDA oligomers of 3, 4, 5 and 6 units successfully using Dowex and amberlyst catalysts (Table 1).

Generally, the reaction of hexose sugar, sorbitol with various aldehydes furnishes the corresponding acetal-based amphiphiles displaying a butterfly-like conformation. The sorbitol moiety is considered as the backbone and the pendant groups attached to it are considered as wings. Bottom-up assembly of butterfly-shaped amphiphiles depends upon the wings, which significantly expand the potential and scope in materials applications. In the current research, the wings were systematically expanded by conjugation with a suitable sorbitol or sorbitol acetals. In an attempt to understand the bottom-up assembly process of the newly synthesized compound HBSD **4**, we have performed gelation studies in a broad range of solvents and vegetable oils. The gelation behaviour of various sorbitol acetals bearing varying degrees of H-bonding and π–π stacking units was studied by the stable to inversion method, which involves the dissolution of the gelator in a suitable solvent by heating followed by cooling to room temperature. While cooling, bottom-up assembly of molecules generates the desired architecture with greater precision and error correction capacity by means of H-bonding and π–π interactions (Table S1, ESI†). Interestingly, these compounds display gelation in polar aprotic solvents such as DMSO, DMF and NMP with the critical gelation concentration (CGC) of 0.6–1.5% (wt/v) (Table S2, ESI†). Representative images of the gel formed in DMSO, DMF and NMP are given in Fig. 1.

NMP is one of the well-known pharmaceutical solvents used for commercial drug formulations. Investigation of the gelation

**Table 1** Optimization for the synthesis of oligo[1,3:2,4-(O-benzylidene)-D-sorbitol]-dialdehyde (OBSDA)

Entry	Catalyst	Mol%	Temp. (°C)	Solvent	Time (h)	DBSD	TBSD (3)	HBSD (4)	OBSD (5)	DBSD (6)	Product/reaction nature
1	AlCl$_3$	0.2	rt	MeCN	12	Traces	31	—	—	—	
2	ZnCl$_2$	0.2	rt	MeCN	12	Traces	45	—	—	—	
3	SnCl$_2$	0.2	rt	MeCN	12	Traces	14	—	—	—	
4	FeCl$_3$	0.2	rt	MeCN	12	Traces	23	—	—	—	
5	BF$_3$.OEt$_2$	0.2	rt	MeCN	12	Traces	62				
6	pTSA	0.2	rt	MeCN	12	Traces	55				
7	H$_3$PO$_4$	0.2	rt	MeCN	12	Traces	Traces				—
8	CH$_3$COOH	0.2	rt	MeCN	12	Traces	Traces				Sluggish
9	HCl	0.2	rt	MeCN	12	—	—				Decomposition
10	Dowex	—	rt	MeCN	12	Traces	72	Traces			
11	Amberlyst	—	rt	MeCN	12	Traces	78	Traces			
12	AlCl$_3$	0.2	50	MeCN	12	Traces	25	12	—	—	
13	ZnCl$_2$	0.2	50	MeCN	12	Traces	32	Traces	—	—	
14	SnCl$_2$	0.2	50	MeCN	12	Traces	Traces	Traces	—	—	
15	FeCl$_3$	0.2	50	MeCN	12	Traces	Traces	Traces	—	—	
16	BF$_3$.OEt$_2$	0.2	50	MeCN	12	Traces	52	16			
17	pTSA	0.2	50	MeCN	12	Traces	38	23			
18	H$_3$PO$_4$	0.2	50	MeCN	12	Traces	Traces				—
19	CH$_3$COOH	0.2	50	MeCN	12	Traces	Traces				Sluggish
20	HCl	0.2	50	MeCN	12	—	—				Decomposition
21	Dowex	—	50	MeCN	12	Traces	63	17			
22	Amberlyst	—	50	MeCN	12	Traces	59	15			
23	Dowex	—	70	MeCN	12	Traces	45	36			
24	Amberlyst	—	70	MeCN	12	Traces	39	40			
25	Dowex	—	Reflux	MeCN	12	Traces	35	42	Traces		
26	Amberlyst	—	Reflux	MeCN	12	Traces	31	48	Traces		
27	Dowex	—	Reflux	MeCN	16	Traces	16	53	Traces		
28	Amberlyst	—	Reflux	MeCN	16	Traces	24	57	Traces		
29	Dowex	—	Reflux	MeCN	20	Traces	Traces	64	Traces		
30	Amberlyst	—	Reflux	MeCN	20	Traces	Traces	67	Traces		
31	Dowex	—	Reflux	MeCN	24		Traces	77	Traces	Traces	
32	Amberlyst	—	Reflux	MeCN	24		Traces	79	Traces	Traces	
33	Dowex	—	Reflux	MeCN	32			65	Traces	Traces	
34	Amberlyst	—	Reflux	MeCN	32			59	Traces	Traces	
35	Dowex	—	Reflux	MeCN	60			18	37	Traces	
36	Amberlyst	—	Reflux	MeCN	60			16	45	Traces	
37	Dowex	—	Reflux	MeOH	60			18	21	Traces	
38	Amberlyst	—	Reflux	MeOH	60			16	27	Traces	
39	Dowex	—	Reflux	Cyrene	60				67	13	
40	Amberlyst	—	Reflux	Cyrene	60				72	11	

behaviour of compounds **3–6** revealed that the tuning of the wing portion by conjugation with benzylidene sorbitol influences the gelation behaviour and assembly pattern. Furthermore, compounds **3–6** were insoluble in most of the non-polar solvents and vegetable oils, whereas a complete or partial dissolution was observed in polar protic solvents. To our fortune, compounds **3–6** displayed excellent gelation in polar aprotic solvents such as DMSO, DMF and NMP. The use of a mixture of solvents such as DMSO, DMF and NMP along with water in a 1 : 1 ratio for the gelation studies substantially alters the intermolecular interactions, and thereby molecules failed to form a supramolecular architecture by means of a bottom-up assembly process. These results clearly reveal that while forming the gel, the introduction of a proton donor interferes with the molecular aggregation, which results in precipitation. At this point, this class of molecules is prone to form a gel in a specific range of solvents, where it can achieve dissolution as a result of intermolecular interactions and solvent balancing in
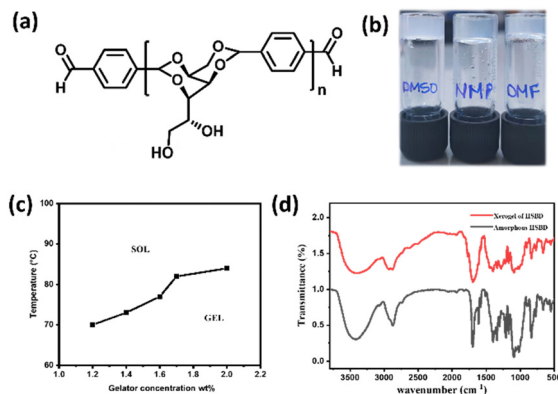
Fig. 1 (a) Butterfly conformation of the gelator; (b) images of a gel formed by HBSD in DMSO, NMP, and DMF solvents (i)–(iii); (c) phase diagram of the HBSD gel formed in NMP with respect to the concentration of gelator in wt/v%. (d) FTIR spectra of HBSD in the xerogel and amorphous state.

Fig. 2 Variable temperature ^{1}H-NMR spectra of the gel formed by HBSD in DMSO-d_6. The shift of proton peaks is highlighted in the blue box.

the bottom-up assembly process. Among the various solvents displaying gelation, NMP is widely used in various industries and pharmaceuticals, and in particular, it is a versatile water-miscible polar aprotic solvent displaying drug solubilization and penetration in humans and animals. The NMP solvent exhibits a well-established safety profile and anti-inflammatory properties.[44,50] Hence, our further research focuses on the gel formed in a pharmaceutical solvent, NMP. Purisol is a physical absorption process employed in chemical industries to remove H_2S and CO_2 from various natural gas streams, crude oil, etc., by using NMP solvent. The high absorption capacity and high boiling point of the NMP solvent allow the removal of acid gases at high pressure and high temperature. A literature review revealed that the Purisol process utilizing NMP is one of the important methods adopted for the purification of syngas at high pressure because of its high selectivity towards H_2S. By gaining clues from the literature, we have encapsulated H_2S into a gel matrix and studied its release profile.

It is worth mentioning that the organogel formed by HBSD **4** is stable under heating and cooling cycles from rt to 70 °C. Heating the gel above 120 °C resulted in precipitation, which is attributed to the cleavage of the acetal moiety of HBSD **4**. The existence of intermolecular interactions in the process of self-assembly can be studied by using Fourier transform infrared spectroscopy (FTIR), X-ray diffraction (XRD), and nuclear magnetic resonance (NMR) studies. FTIR spectroscopy provides insights into various molecular interactions that give rise to self-assembled 3D supramolecular architectures. The FTIR spectrum of amorphous HBSD and HBSD xerogels in NMP solvent is shown in Fig. 1. HBSD in an amorphous state displays O–H stretching vibrations at 3428 cm^{-1} and aldehyde carbonyl (C=O) stretching at 1699 cm^{-1}. After undergoing self-assembly in NMP solvent, the HBSD xerogels displayed O–H stretching vibrations at 3410 cm^{-1}, and aldehyde (C=O) stretching at 1695 cm^{-1}, which implies the involvement of hydroxy groups and aldehyde carbonyl groups in the process of H-bonding-mediated self-assembly of molecules into 3D architectures.
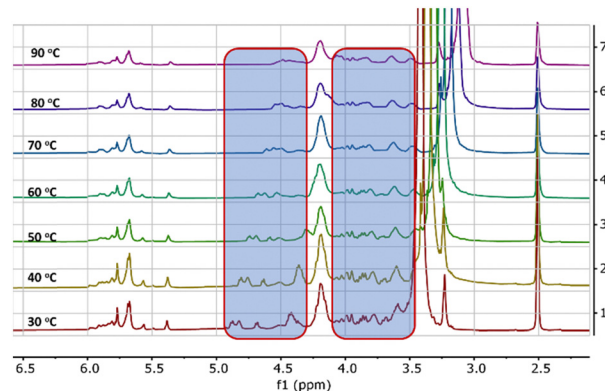
Further evidence of the self-assembly process is probed from variable temperature ^{1}H-NMR spectral studies. ^{1}H-NMR of HBSD in DMSO at various temperatures is displayed in Fig. 2. Variable temperature ^{1}H-NMR spectral studies revealed that upon increase in temperature, an upfield shift in signals corresponding to the proton of the methylene and free hydroxy groups from δ = 4.84, 4.68, 4.41 ppm to δ = 4.41, 4.30 and 4.05 was observed. In a complex system like carbohydrates, it is very difficult to understand the electronic nature of various groups in free and assembled states. In the assembled state, because of the involvement of –OH groups in intermolecular H-bonding, the electron density decreases and hence the respective proton generates a relatively lower induced magnetic field. Owing to the consequences of the induced magnetic field, the protons of methylene and hydroxyl groups feel a higher magnitude of the applied magnetic field and hence relatively higher frequency is required for the resonance. However, upon disassembly, these protons display an upfield shift because of the disturbance in the intermolecular interaction. Increased electron density in the aggregated π-conjugated systems is fairly known in the literature, which is considered as one of the basic criteria for the development of organic electrons and sensors. However, the influence of aggregation in the σ-system is not known to date, and such investigations are very important to study the structure-function activity of complex biological systems. VT ^{1}H-NMR studies revealed that upon molecular assembly, the CH protons of the carbohydrate moiety resonated at lower frequencies and upon gel-to-sol transition influenced by the heating displayed a downfield shift in protons (Fig. 2). This demonstrates the involvement of hydroxy groups in the self-assembly process by means of H-bonding.

The mechanical characteristics of the HBSD gel formed in NMP were investigated by studying its viscoelastic properties using a rheometer. Gels undergo deformation in response to stress or strain, which depends upon the intermolecular interactions governing the supramolecular architecture. Investigation of the flow characteristics of gel with respect to strain amplitude sweep and angular frequency sweep in terms of storage modulus(G') and loss modulus(G'') is very crucial for biomedical applications. In Fig. 3, throughout the frequency
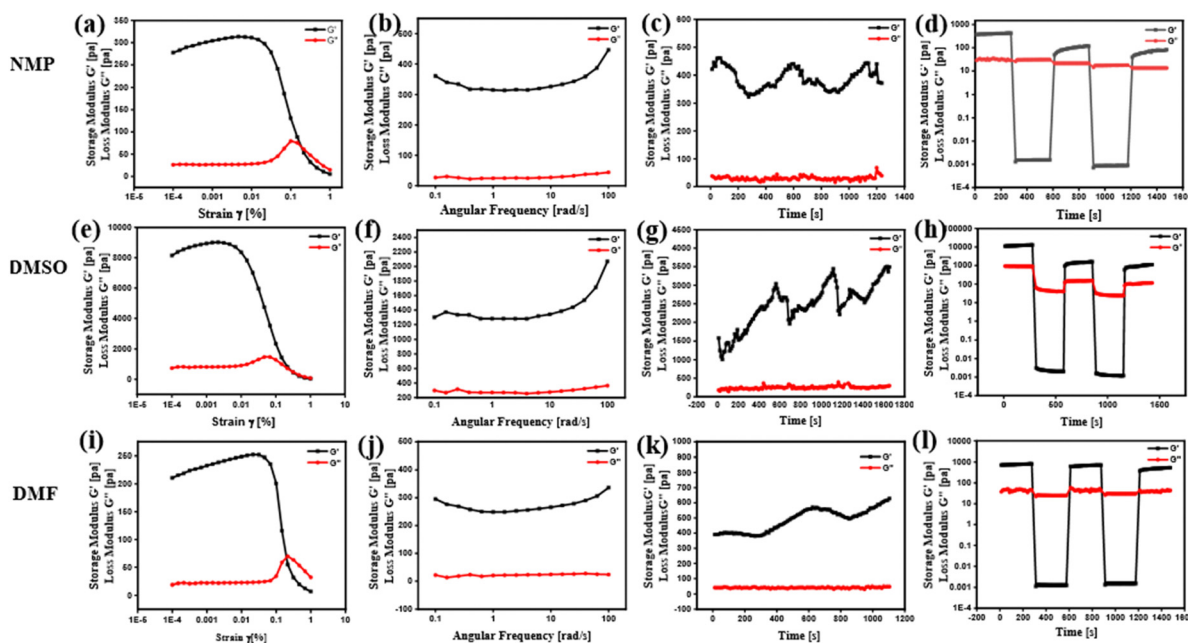
Fig. 3 Frequency sweep, amplitude sweep, thixotropy and temperature ramp up studies of the HBSD gel formed in NMP (a)−(d), DMSO (e)−(h) and DMF (i)−(l), respectively.

sweep measurements of the HBSD gel, it was consistently observed that the storage modulus G' remained higher than the loss modulus G''; this indicates that the HBSD gel exhibits stability and resilience towards external forces. The amplitude sweep measurements distinctly demonstrate that the HBSD gels show gel-like behaviour ($G' > G''$) up to a critical strain level of 0.02%. After this point, a decrease in G' and G'' indicates the onset of fluid-like behaviour in the gels. After assessing the gel's capacity to endure external forces, we proceeded to evaluate the processability of the gels through continuous temperature ramp-up and ramp-down experiments conducted within the temperature range of 23 °C to 45 °C. This study demonstrates that these gels undergo disassembly upon heating and then reassemble the gel network upon cooling, driven by reversible non-covalent interactions. Typically, the thixotropic nature of the gels provides insight into their capacity to restore the structural integrity that may have been compromised due to the application of different strains to the gel. After applying a constant strain of 100%, the HBSD gel experienced a reduction in strength. However, upon decreasing the strain to 0.1%, the viscosity of the gels returned to the initial state. Through a sequence of three successive cycles of continuous strain ramp-up and ramp-down experiments, we observed a gradual deterioration in gel structural integrity as the strain increased. However, the original state promptly recovered as the strain was eased back to 0.1%.

During the process of self-assembly, the way in which individual molecules are interconnected to create well-ordered 3D architectures such as fibers, tubules, helices, lamellae, twisted fibers, micelles, and vesicles is of utmost significance. These organized patterns contributed distinctive attributes to the resulting soft materials. Scanning electron microscopy is
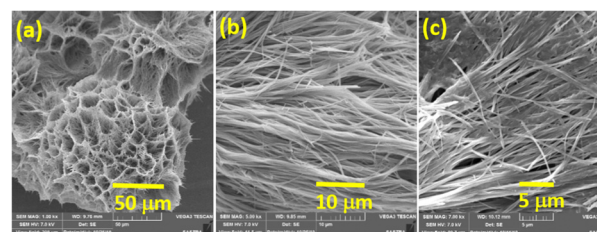

Fig. 4 SEM images of xerogels of HBSD in NMP at (a) 50 μm, (b) 10 μm and (c) 5 μm.

employed to investigate the morphology of the self-assembled gels. Fig. 4 shows that HBSD gels in NMP display fibre like structures in the self-assembled state.

Regardless of its foul-smelling and toxic nature, H_2S is an important gasotransmitter in the neurosystem. Initially the biological properties of H_2S were investigated by direct administration of NaHS and Na_2S, but the main drawback in direct administration is the rapid increase in the concentration of H_2S and then it declines rapidly, which causes an inflammatory response. The development of H_2S based drugs is quite challenging because of its volatility and rapid metabolism. Hence, a controlled H_2S delivery system is necessary. Regulation of H_2S delivery has become a prominent area for research since the last few decades. Many types of drug delivery systems from complex macromolecular architectures to nanofiber systems have been used to deliver H_2S. Among these drug delivery systems, gels have attracted a wide range of interest because of their 3D-porous network, biodegradability, and stimuli responsive gel–sol transition. In a recent study, Arunan and his colleagues utilized microwave spectroscopy to confirm the existence of hydrogen bonding in H_2S,[51] which made us curious

to establish a new method to encapsulate H_2S through an *in situ* gelation process.

By considering its solubility with H_2S gas, we have engineered a drug delivery protocol in which H_2S is directly injected into a solution of HBSD dissolved in NMP. This results in a self-assembly process that leads to gel formation, effectively entrapping the H_2S gas. Entrapment of H_2S is greater in HBSD gel formed in NMP because of dipole–dipole interaction, acid–base interaction, and size and polarizability of H_2S with NMP, in addition to the complementary H-bonding extended by the gelator and NMP. Injecting H_2S into HBSD solution in NMP has accelerated the self-assembly process and gel formed quickly. The entrapment of H_2S can be visually confirmed by the colour change of the HBSD gel from white to yellow. To investigate the self-assembly mechanism after the injection of H_2S, we have recorded FTIR spectra for the xerogel of HBSD before and after injection of H_2S (Fig. 5a). In the FTIR spectra, the peak observed at 2602 cm^{-1} represents the S–H stretching frequency, confirming the encapsulation of H_2S in the gel matrix, which is absent in the HBSD xerogel. A comparison of O–H stretching vibrations in HBSD and H_2S encapsulated xerogels revealed the engagement of hydroxyl groups in H-bonding with H_2S. It is worth mentioning that the increase in H-bonding with H_2S substantially increases the strength of the gels, which is clearly demonstrated by angular frequency and amplitude sweep experiments (Fig. 5c and d). The storage modulus of the H_2S encapsulated gel is higher than the storage modulus of HBSD gel, implying an increase in the strength of the gel upon forming H-bonding with H_2S.

Molecular packing of HBSD and H_2S encapsulated gels was identified using XRD analysis and the HBSD xerogels displayed peaks at $2\theta = 8.28, 10.80, 12.5, 19.29, 22.10, 23.59, 32.97, 34.29, 28.36, 36.48$ and 48.19, corresponding to the d-spacing (interplanar spacing) of 10.66, 8.17, 7.15, 4.59, 4.01, 3.76, 2.71, 2.61, 3.14, 2.46 and 1.88 nm, respectively. However, xerogels of HBSD-H_2S displayed peaks at $2\theta = 8.85, 11.79, 19.37, 22.08$,

23.63, 32.97, 34.30, 47.03, 47.51 and 48.24, which correspond to the d-spacing of 9.97, 7.49, 4.57, 4.021, 3.76, 2.71, 2.61, 1.93, 1.91 and 1.88 nm, respectively. The notable variation in the d-spacing of the molecular structures, observed before and after H_2S injection, provides strong evidence for the interaction between H_2S and HBSD (Fig. 5b).

Having established the interactions of H_2S in the HBSD gel, we have investigated the stability of these gels at different pH conditions. Initial H_2S release studies at neutral pH displayed the stability of the HBSD gel towards distilled water. It is worth mentioning that a little release of H_2S is observed because of the exchange of entrapped NMP in the HBSD gel by water molecules rather than a rapid disintegration. It is observed that at pH = 4.0, the gel slowly disintegrates and releases H_2S, whereas at neutral and basic pH levels, the gel retains its stability. Having obtained an interesting result, we were curious to propose a plausible mechanism. Visual observation and NMR spectral studies revealed that the release of H_2S is due to disruption of H-bonding, visualized by the conversion of the translucent gel into an opaque soft gel and the slow hydrolysis of acetal groups present in the HBSD gelator, which in turn collapses the structural integrity of the self-assembled fibrillar network. During the process of disassembly of the H_2S entrapped HBSD gel, H_2S gas trapped in the fibrillar network is released. Acetyl-based gels have great potential in controlled delivery of drugs and active pharmaceutical ingredients. As shown in Fig. 6, when a buffer solution of pH 4.0 is added on top of the HBSD-H_2S gel, disassembly of the gel occurs, and thereby gradual release of H_2S is observed. The deformation of the gel with a significant colour change in buffer solution is physically visible; however, the release of H_2S is systematically assessed by converting it into the respective metal sulphides. It is well known that under normal room temperature, the interaction between various metal ions and H_2S often gives rise to the formation of the corresponding metal sulfides. Specifically, group II cations exhibited a tendency to form less soluble
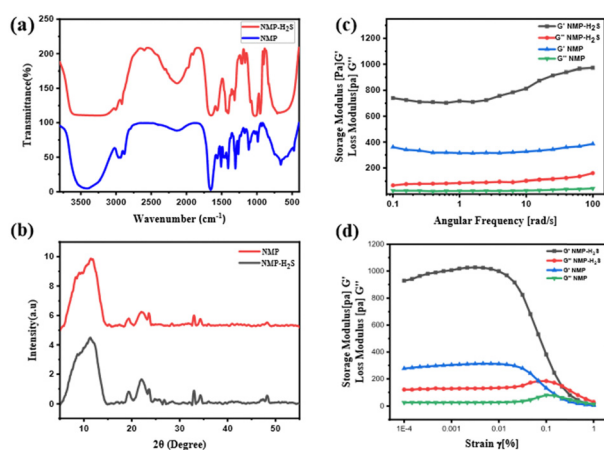
Fig. 5 (a) FTIR spectra of the HBSD xerogel and H_2S encapsulated gel; (b) XRD of xerogels of HBSD in NMP before and after loading H_2S; (c) and (d) a comparative rheology of HBSD gel formed in NMP and H_2S encapsulated gel, respectively.
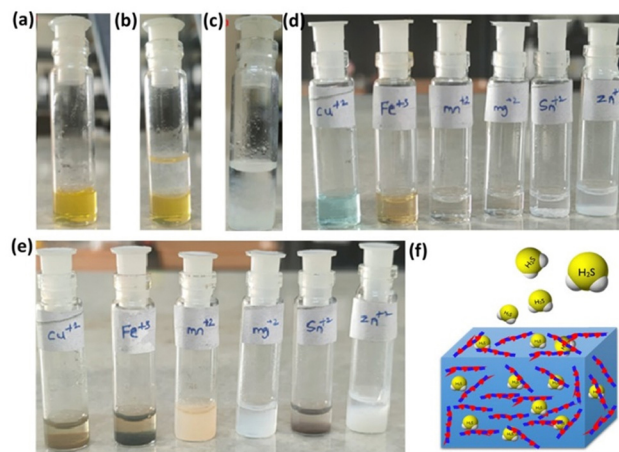
Fig. 6 (a) H_2S entrapped gel. (b) H_2S entrapped gel in acidic medium (pH-4.0). (c) H_2S entrapped gel in acidic medium after 12 h (d). Different metal ion solutions. (e) Metal sulfides formed after the addition of released H_2S. (f) Pictorial representation of H_2S release from the HSBD gel.
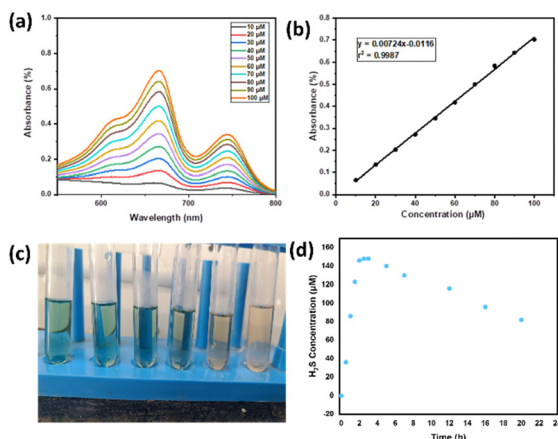
Fig. 7 (a) Methylene blue assay at different concentrations of Na_2S. (b) Linear regression analysis of concentration *vs.* absorbance. (c) Photograph of the formation of methylene blue by the released H_2S from the HBSD gel at different time intervals. (d) H_2S release profile displayed by HBSD gel at different time intervals.

metal sulfides (with a solubility product constant, Ksp, of less than 10^{-30}) when exposed to lower amounts of H_2S. After the addition of buffer solution of pH 4.0, the supernatant liquid is retrieved and further added to a vial containing a solution of different metal ions such as Cu^{2+}, Fe^{3+}, Mn^{2+}, Mg^{2+}, Sn^{2+} and Zn^{2+} at 0.1 M concentration. The minimum concentration of H_2S present in the aliquots reacting with the respective metal ions in turn generated an insoluble metal sulphide, which was confirmed by the change in colour (Fig. 6). In order to quantify the loaded H_2S in the HBSD gel and their release profile, a linear regression analysis is performed by taking the absorbance values obtained from a methylene blue assay (Fig. 7a and b).[53] To 1 mL of H_2S entrapped HBSD gel, pH = 4 buffer solution is added, and aliquots of 0.5 mL are collected at 30-minute intervals and a methylene blue assay is performed. The interpolation of the obtained UV data with the linear regression plot revealed a slow release of H_2S with respect to time and reached a maximum release after 3 h. It is worth mentioning that a slow fall in the H_2S concentration is observed because of its volatility. The total amount of H_2S loaded in the gel is observed as 148 μm. In contrast to other H_2S donors or H_2S delivery materials documented in the literature, the reported smart gel offers numerous advantages, such as uncomplicated encapsulation of H_2S in the gel without necessitating any covalent bonding, achieved through a self-assembly mechanism. There is no requirement for additional H_2S donors. Furthermore, the HBSD gel exhibits pH-triggered H_2S delivery.

Experimental

General materials and methods

All reagents and solvents used for the synthesis of diformyl dibenzylidene sorbitol were purchased from commercial suppliers such as Merck, Aldrich, Himedia and Avra chemicals and

were used without purification. We have used LR grade solvents for recrystallization and AR grade solvents for gelation studies. The progress of the reactions was monitored by thin-layer chromatography (TLC) using pre-coated Merck silica gel 60 F254 plates and visualized by UV detection or using sulfuric acid spray or molecular iodine. Melting points were recorded on Stuart SMP30 melting point apparatus in capillaries and are uncorrected. ^1H- and ^{13}C-NMR spectra were recorded on a Bruker Avance 300 MHz instrument in deuterated solvents such as D_2O, DMSO-d_6, $CDCl_3$, and $CDCl_3$ with a few drops of DMSO-d_6 at room temperature. TMS is used as an internal standard and chemical shifts in NMR spectra (δ) are reported in parts per million (ppm). Multiplicity in the ^1H NMR spectra of the synthesized compounds was referred to as singlet (s), doublet (d), triplet (t), quartet (q) and multiplet (m), and coupling constants (J) are given in Hz. Infrared (IR) spectra were recorded using a PerkinElmer spectrum 100 spectrophotometer from 400–4000 cm^{-1} using KBr. High resolution MS analysis was performed on an Agilent Q-TOF 6230 instrument by dissolving the solid sample in methanol or acetonitrile. To obtain the morphology of the gel, scanning electron microscopy is used with a JEOL JSM-6701F ultrahigh resolution field emission scanning electron microscope. The XRD measurements were taken by keeping a small portion of the xerogel in the X'pert-PRO Diffractometer system.

General procedure for the synthesis of HBSD oligomers

To a stirred solution of D-sorbitol (1 mmol) in acetonitrile (10 mL) at rt under N_2 atmosphere, terepthaldehyde (2 mmol) and Dowex 50WX8/Amberlyst were added. The reaction mixture was stirred for another 24 h under reflux conditions. After completion of the reaction confirmed by TLC, the reaction mixture was allowed to cool down to room temperature. The formed precipitate is dissolved in hot cyrene and separates the catalyst by filtration. The cyrene solution is refrigerated for crystallization. The catalyst was further reused in other reactions.

TSBD(3). white solid; yield: 78%; ^1H NMR (400 MHz, DMSO) δ 10.04 (s, 2H, C$\underline{H}$O), 7.95 (d, J = 6.4 Hz, 4H, Ar$\underline{H}$), 7.70 (t, J = 8.6 Hz, 4H, Ar$\underline{H}$), 7.57–7.42 (m, 4H, Ar$\underline{H}$), 6.03–5.65 (m, 4H, C$\underline{H}$(OR)$_2$), 4.97–4.81 (m, 1H), 4.60–4.32 (m, 3H), 4.30–4.10 (m, 6H), 4.09–3.95 (m, 2H), 3.94–3.84 (m, 1H), 3.80 (s, 1H), 3.62 (d, J = 4.9 Hz, 1H), 3.49 (dt, J = 11.9, 5.9 Hz, 1H), 3.67–3.52 (m, 1H), 3.29–3.16 (m, 3H); ^{13}C NMR (101 MHz, DMSO) δ 193.45, 144.66, 137.23, 136.75, 130.48, 129.78, 127.82, 127.36, 126.29, 102.56, 99.54, 98.99, 78.05, 69.81, 69.02, 68.10, 63.03, 48.96, 30.58, 29.48, 17.69. ESI-MS: m/z calculated for $C_{36}H_{38}O_{14}$ $[M + Na]^+$ is 717.2159: found m/z = 717.2135.

HBSD(4). white solid; yield 79%; ^1H NMR (400 MHz, DMSO) δ: 10.03 (s, 2H, C$\underline{H}$O), 7.94 (d, J = 7.8 Hz, 4H, Ar$\underline{H}$), 7.77–7.65 (m, 4H, Ar$\underline{H}$), 7.58–7.38 (m, 8H, Ar$\underline{H}$), 5.99–5.75 (m, 3H, C$\underline{H}$(OR)$_2$), 5.74–5.63 (3, 3H, C$\underline{H}$(OR)$_2$), 4.59–4.09 (m, 8H), 4.07–3.94 (m, 2H), 3.93–3.82 (m, 2H), 3.82–3.73(m, 2H), 3.72–3.52(m, 4H), 3.52–3.37 (m, 9H), 3.26–3.14(m, 3H); ^{13}C NMR (101 MHz, DMSO) δ: 193.44, 145.00, 136.80, 129.87, 129.79, 127.39, 126.28, 102.81, 99.56, 78.12, 70.55, 69.59, 68.91, 68.14, 63.04.

ESI-MS: m/z calculated for $C_{50}H_{54}O_{20}$ $[M + Na]^+$ is 997.3101: found m/z = 997.3100.

OBSD(5): white solid; yield: 72%; ^1H NMR (400 MHz, DMSO) δ 10.03 (s, 2H, C$\underline{H}$O), 7.94 (d, J = 7.9 Hz, 4H, Ar$\underline{H}$), 7.70 (q, J = 7.1 Hz, 4H, Ar$\underline{H}$), 7.59–7.36(m, 12H, Ar$\underline{H}$), 6.00–5.89 (m, 1H, C$\underline{H}$(OR)$_2$), 5.83 (d, J = 10.9 Hz, 1H, C$\underline{H}$(OR)$_2$), 5.77 (s, 1H, C$\underline{H}$(OR)$_2$), 5.69 (q, J = 6.8 Hz, 4H, C$\underline{H}$(OR)$_2$), 5.60–5.44 (m, 1H, C$\underline{H}$(OR)$_2$), 4.52 (s, 1H), 4.38 (s, 1H), 4.19 (q, J = 11.6 Hz, 10H), 4.05–3.94 (m, 4H), 3.90–3.74 (m, 6H), 3.73–3.65 (m, 2H), 3.59 (m, 6H), 3.45 (m, 9H), 3.17(s, 1H).

DBSD(6). white solid; yield: 13%; ^1H NMR (400 MHz, DMSO) δ 10.03 (s, 2H, C$\underline{H}$O), 7.94 (d, J = 7.0 Hz, 4H, Ar$\underline{H}$), 7.69 (t, J = 8.3 Hz, 4H, Ar$\underline{H}$), 7.60–7.35 (m, 16H, Ar$\underline{H}$), 6.00–5.33 (m, 10H, C$\underline{H}$(OR)$_2$), 4.94–4.80 (m, 2H), 4.74–4.63 (m, 1H), 4.50–4.22 (m, 6H), 4.27–4.09 (m, 13H), 4.07–3.92 (m, 5H), 3.92–3.73 (m, 6H), 3.69 (d, J = 11.4 Hz, 1H), 3.59 (s, 4H), 3.54–3.46 (m, 6H), 3.23 (s, 6H).

Gelation studies. To a known quantity of HBSD taken in a test tube, the appropriate amount of solvent was added and sealed tightly, and the system was heated until the solid gets completely dissolved. The homogeneous solution thus obtained was allowed to cool slowly to rt. The gelation ability of HBSD can be observed by the naked eye by inverting the test tube. In the inverted test tube, a sample exhibiting no gravitational flow is referred as a gel "G"; if instead it remains as a solution it is referred to as "S". If the compound is insoluble, it is referred to as "I". Precipitation and crystallization observed in the test tube is denoted as "P" and "Crys" respectively. Amphiphilic C-glycosyl furan displaying insoluble nature even at the boiling point of the solvent is referred to as "I".

Morphological analysis. The morphology of the HBSD gel was studied using a Carl Zeiss AXIO ScopeA1 fluorescent/phase contrast microscope, JEOL JSM-6701F ultrahigh resolution field emission scanning electron microscope and JEOL JEM 2100F FETEM. In order to analyse the morphology of HBSD gel, a small portion of hydrogel is placed on a glass slide and subjected to a Phase Contrast Microscope. For FETEM analysis, 10 mL of water is added to 3 mg of gel taken in a vial, followed by sonication for 1 min. After sonication, fibers in the gel were dispersed and the morphology of the dispersed fibers was analyzed by FETEM.

Rheological measurements. The thermal, mechanical and thixotropic behaviour of HBSD gel was identified using an Anton Paar 302 rheometer. Experiments were carried with a 25 mm diameter steel-coated parallel-plate geometry, where a 1 mm gap between two plates was maintained. The linear viscoelastic range was identified by performing amplitude sweep measurement, which is directly proportional to the mechanical strength of the gel sample. The storage modulus, G′ and the loss modulus, G″ of HBSD gel as functions of frequency sweep were also performed at 23 °C.

Encapsulation of H$_2$S. Na$_2$S flakes are taken into a double neck round bottom flask fitted with a rubber septum. Into the round bottom flask, 40% H$_2$SO$_4$ is added through a glass syringe. When H$_2$SO$_4$ is reacted with Na$_2$S, it generates H$_2$S gas. The released gas is trapped in a rubber balloon attached to the round bottom flask through a syringe. Then, the H$_2$S gas is injected directly into the HBSD solution in NMP and left to form a gel.

Methylene blue assay. In order to quantify the loaded H$_2$S in the HBSD gel and their release profile, a standard plot was arrived at by preparing 1.0 mM Na$_2$S as a stock solution. 5 mL of Na$_2$S at varying concentrations ranging from 10 to 100 μM was prepared from the stock solution. Samples for the assay are prepared by taking 0.5 mL of each concentration of Na$_2$S solution and mixing it with 0.5 mL of FeCl$_3$ solution, followed by 0.5 mL of N,N-dimethylphenylene diamine sulfate solution. The samples are incubated at room temperature for 3 h, and the absorbance of each sample is recorded using a UV-vis spectrometer.[52] During this process, the formation of methylene blue displayed absorbance at 667 nm, and the intensity increased with the increase in the concentration of Na$_2$S. Linear regression analysis is performed by taking the absorbance values at 667 nm.[53] The quantification of H$_2$S release from the HBSD gel has been performed in duplicate. To the H$_2$S entrapped HBSD gel, pH = 4 buffer solution is added, and aliquots of 0.5 mL are collected at 30-minute time intervals. To these aliquots, 0.5 mL of FeCl$_3$ solution, followed by 0.5 mL of N,N-dimethylphenylene diamine sulfate solution, was added and incubated for 3 h at room temperature. The formation of methylene blue was confirmed by the absorbance at 667 nm using UV-vis spectroscopy and interpolated with the linear regression plot to obtain the concentration of H$_2$S released at different time intervals.

Conclusions

In summary, we have synthesized oligo[1,3:2,4-(O-benzylidene)-D-sorbitol]-dialdehyde (OBSDA) using an environmentally benign protocol in good yields. Supramolecular gelation of HBSA, one of the OBSDA compounds, displayed gelation in FDA-approved pharmaceutical solvents, N-methyl pyrrolidone (NMP). Molecular level interactions such as H-bonding and π–π stacking responsible for the formation of a supramolecular architecture have been identified using NMR and FTIR analysis. Morphology and mechanical strength analysis clearly establish the suitability of the gel for pharmaceutical applications. Owing to the volatile nature of H$_2$S, to date researchers have utilized additional H$_2$S donors in fabricating drug delivery systems. This report deals with the direct encapsulation of H$_2$S gas into a gel matrix and stimuli responsive delivery via gel-to-sol transition, clearly demonstrating the suitability of NMP gel in evaluating the physiological role of H$_2$S in various biological processes. It also has scope in transdermal drug delivery applications, as NMP has high penetrating capacity through the skin.

Conflicts of interest

There are no conflicts to declare.

Acknowledgements

Notes and references

1 F. Huang and E. V. Anslyn, *Chem. Rev.*, 2015, **115**, 6999–7000.

2 B. X. Jie Zhou, J. Li and X. Du, *Biomaterials*, 2017, **129**, 1–27.

3 A. Hardenia, N. Maheshwari, S. S. Hardenia, S. K. Dwivedi, R. Maheshwari and R. K. Tekade, *Scientific rationale for designing controlled drug delivery systems*, Elsevier Inc., 2018, pp. 1–28.

4 D. Yadav, K. Sandeep, D. Pandey and R. K. Dutta, *J. Biotechnol. Biomater.*, 2017, **7**, 276.

5 H. S. Kapare and S. R. Metkar, *Pharm. Reson.*, 2020, **2**, 21–26.

6 A. Z. Wilczewska, K. Niemirowicz, K. H. Markiewicz and H. Car, *Pharmacol Rep.*, 2012, **64**, 1020–1037.

7 E. Chappel, *Implantable drug delivery devices*, Elsevier Inc., 2021, pp. 129–156.

8 W. B. Liechty, D. R. Kryscio, B. V. Slaughter and N. A. Peppas, *Annu. Rev. Chem. Biomol. Eng.*, 2010, **1**, 149–173.

9 Z. Li, J. Cao, H. Li, H. Liu, F. Han, Z. Liu, C. Tong and S. Li, *Drug Delivery*, 2016, **23**, 3168–3178.

10 E. Beltrán-Gracia, A. López-Camacho, I. Higuera-Ciapara, J. B. Velázquez-Fernández and A. A. Vallejo-Cardona, *Nanomedicine review: Clinical developments in liposomal applications*, Springer Vienna, 2019, vol. 10.

11 R. K. Thapa and J. O. Kim, *J. Pharm. Investig.*, 2023, **53**, 19–33.

12 S. H. Roth, *Signal Transduction Gasotransm.*, 2004, 293–313.

13 K. Abe and H. Kimura, *J. Neurosci.*, 1996, **16**, 1066–1071.

14 R. Wang, *FASEB J.*, 2002, **16**, 1792–1798.

15 A. Katsouda, S.-I. Bibli, A. Pyriochou, C. Szabo and A. Papapetropoulos, *Pharmacol. Res.*, 2016, **113**, 175–185.

16 D. Wu, N. Luo, L. Wang, Z. Zhao, H. Bu, G. Xu, Y. Yan, X. Che, Z. Jiao, T. Zhao, J. Chen, A. Ji, Y. Li and G. D. Lee, *Sci. Rep.*, 2017, **7**, 455.

17 R. C. O. Zanardo, V. Brancaleone, E. Distrutti, S. Fiorucci, G. Cirino, J. L. Wallace, R. C. O. Zanardo, V. Brancaleone, E. Distrutti, S. Fiorucci, G. Cirino and J. L. Wallace, *FASEB J.*, 2006, **20**, 2118–2120.

18 R. Wang, *Physiol. Rev.*, 2012, **92**, 791–896.

19 D. J. Lefer, *Proc. Natl. Acad. Sci. U. S. A.*, 2007, **104**, 17907–17908.

20 C. Hine, E. Harputlugil, Y. Zhang, C. Ruckenstuhl, B. C. Lee, L. Brace, A. Longchamp, J. H. Treviño-Villarreal, P. Mejia, C. K. Ozaki, R. Wang, V. N. Gladyshev, F. Madeo, W. B. Mair and J. R. Mitchell, *Cell*, 2015, **160**, 132–144.

21 M. Whiteman and P. G. Winyard, *Expert Rev. Clin. Pharmacol.*, 2011, **4**, 13–32.

22 W. Y. Zheng, B. Yu, L. K. De La Cruz, M. R. Choudhury, A. Anifowose and B. Wang, *Med. Res. Rev.*, 2017, **38**, 57–100.

23 A. K. Gilbert and M. D. Pluth, *J. Am. Chem. Soc.*, 2022, **144**, 17651–17660.

24 C. R. Powell, J. C. Foster, B. Okyere, M. H. Theus and J. B. Matson, *J. Am. Chem. Soc.*, 2016, **138**, 13477–13480.

25 W. Wang, X. Sun, H. Zhang, C. Yang, Y. Liu, W. Yang, C. Guo and C. Wang, *Int. J. Nanomed.*, 2016, **11**, 3255–3263.

26 M. K. Marwah, H. Shokr, L. Sanchez-Aranguren, R. K. S. Badhan, K. Wang and S. Ahmad, *Pharm. Res.*, 2022, **39**, 341–352.

27 S. H. Yu, L. Esser, S. Y. Khor, D. Senyschyn, N. A. Veldhuis, M. R. Whittaker, F. Ercole, T. P. Davis and J. F. Quinn, *J. Polym. Sci., Part A: Polym. Chem.*, 2019, **57**, 1982–1993.

28 H. Zhang, L. Z. Hao, J. A. Pan, Q. Gao, J. F. Zhang, R. K. Kankala, S. Bin Wang, A. Z. Chen and H. L. Zhang, *J. Controlled Release*, 2021, **329**, 286–298.

29 A. Longchamp, K. Kaur, D. Macabrey, C. Dubuis, J. M. Corpataux, S. Déglise, J. B. Matson and F. Allagnat, *Acta Biomater.*, 2019, **97**, 374–384.

30 X. Sun, Y. Wang, S. Wen, K. Huang, J. Huang, X. Chu, F. Wang and L. Pang, *J. Nanobiotechnol.*, 2021, **19**, 1–16.

31 L. E. Buerkle and S. J. Rowan, *Chem. Soc. Rev.*, 2012, **41**, 6089–6102.

32 E. R. Draper and D. J. Adams, *Chem*, 2017, **3**, 390–410.

33 K. Kaur, Y. Wang and B. M. John, *Biomacromolecules*, 2020, **21**, 1171–1178.

34 Y. Qian, K. Kaur, J. C. Foster and J. B. Matson, *Biomacromolecules*, 2019, **20**, 1077–1086.

35 Y. Wang, K. Kaur, S. J. Scannelli, R. Bitton and J. B. Matson, *J. Am. Chem. Soc.*, 2018, **140**, 14945–14951.

36 Y. Qian, A. Altamimi, S. A. Yates, S. Sarkar, M. Cochran, M. Zhou, N. Levi-Polyachenko and J. B. Matson, *Biomater. Sci.*, 2020, **8**, 2564–2576.

37 M. Zhou, Y. Qian, Y. Zhu and J. Matson, *Chem. Commun.*, 2020, **56**, 1085–1088.

38 W. Liang, J. Chen, L. Li, M. Li, X. Wei, B. Tan, Y. Shang, G. Fan, W. Wang and W. Liu, *ACS Appl. Mater. Interfaces*, 2019, **11**, 14619–14629.

39 A. Thamizhanban, K. Lalitha, G. P. Sarvepalli, C. U. Maheswari, V. Sridharan, J. B. B. Rayappan and S. Nagarajan, *J. Mater. Chem. B*, 2019, **7**, 6238–6246.

40 J. Wu, A. Chen, Y. Zhou, S. Zheng, Y. Yang, Y. An, K. Xu, H. He, J. Kang, J. A. Luckanagul, M. Xian, J. Xiao and Q. Wang, *Biomaterials*, 2019, 119398.

41 C. R. Powell, K. M. Dillon and J. B. Matson, *Biochem. Pharmacol.*, 2018, **176**, 110–123.

42 B. O. Okesola, M. P. Vieira, D. J. Cornwell, N. K. Whitelaw and D. K. Smith, *Soft Matter*, 2015, **11**, 4768–4787.

43 R. C. Deis and M. W. Kearsley, *Sweeteners and Sugar Alternatives in Food Technology*, 2012, pp. 331–346.

44 A. Jouyban, M. A. A. Fakhree and A. Shayanfar, *J. Pharm. Pharm. Sci.*, 2010, **13**, 524–535.

45 R. B. N. L. Kohl, *Handbook of Natural Gas Transmission and Processing*, 2019, pp. 231–269.

46 E. J. Howe, B. O. Okesola and D. K. Smith, *Chem. Commun.*, 2015, **51**, 7451–7454.

47 C. C. Piras, A. K. Patterson and D. K. Smith, *Chem. – Eur. J.*, 2021, **27**, 13203–13210.

48 K. Peng, T. Sottmann and C. Stubenrauch, *Mol. Phys.*, 2021, **119**, 15–16.

49 B. Springs, C. Xie and J. Xia, US 2006/0079720 A1, 2006.

50 M. Roche-Molina, B. Hardwick and C. Sanchez-Ramos, *et al.*, *Sci. Rep.*, 2020, **10**, 11636.

51 A. Das, P. K. Mandal, F. J. Lovas, C. Medcraft, N. R. Walker and E. Arunan, *Angew. Chem., Int. Ed.*, 2018, **57**, 15199–15203.

52 J. C. Foster, S. C. Radzinski, X. Zou, C. V. Finkielstein and J. B. Matson, *Mol. Pharmaceutics*, 2017, **14**, 1300–1306.

53 S. Feng, Y. Zhao, M. Xian and Q. Wang, *Acta Biomater.*, 2015, **27**, 205–230.